

## Research Article

# The Benzylolation of *p*-Xylene Using $\text{ZnFe}_2\text{O}_4$ Nanoparticles as Heterogeneous Catalyst

Nguyen Le My Linh,<sup>1</sup> Ho Thi Bao Giang,<sup>1</sup> Le Quoc Thang,<sup>1</sup> Tran Dong Tien,<sup>1</sup>  
Nguyen Thi Anh Thu,<sup>1</sup> Tran Duong,<sup>1</sup> Hoang Van Duc,<sup>1</sup> Le Thi Hoa,<sup>2</sup> Vo Thang Nguyen,<sup>3</sup>  
Dao Ngoc Nhiem ,<sup>4</sup> and Dinh Quang Khieu <sup>2</sup>

<sup>1</sup>University of Sciences, Hue University, 530000, Vietnam

<sup>2</sup>University of Education and Science, The University of Da Nang, 500000, Vietnam

<sup>3</sup>Institute of Materials Science, VAST, 100000, Vietnam

<sup>4</sup>University of Education, Hue University, 530000, Vietnam

Correspondence should be addressed to Dinh Quang Khieu; dqkhieu@hueuni.edu.vn

Received 6 November 2021; Revised 25 February 2022; Accepted 22 March 2022; Published 4 April 2022

Academic Editor: Palanivel Velmurugan

Copyright © 2022 Nguyen Le My Linh et al. This is an open access article distributed under the Creative Commons Attribution License, which permits unrestricted use, distribution, and reproduction in any medium, provided the original work is properly cited.

In this paper,  $\text{ZnFe}_2\text{O}_4$  nanomaterial synthesized in different solvents by hydrothermal method was used as catalyst for the benzylolation of *p*-xylene.  $\text{ZnFe}_2\text{O}_4$  catalyst was characterized by XRD, EDX, SEM and nitrogen adsorption/desorption isotherms. The influence of various parameters in the benzylolation of *p*-xylene such as the Fe content of the prepared materials, the ratio molar of *p*-xylene/benzyl chloride, the catalyst dosage, and the temperature was investigated. The relationship between adsorption kinetics and reaction kinetics of *p*-xylene benzylolation over  $\text{ZnFe}_2\text{O}_4$  nanoparticles was discussed. The results indicated that  $\text{ZnFe}_2\text{O}_4$  catalyst synthesized in ethylene glycol (ZFO-EG) showed high conversion for the benzylolation of *p*-xylene. The reusability of the ZFO-EG catalyst was also investigated.

## 1. Introduction

The Friedel-Crafts reaction is considered as one of the most important reactions in organic synthesis, particularly the benzylolation of aromatic compounds with homogeneous Lewis acid catalysts. There are many disadvantages of using homogeneous catalysts such as  $\text{AlCl}_3$ ,  $\text{H}_2\text{SO}_4$ , and  $\text{H}_3\text{PO}_4$  solutions including side reactions (polyalkylation or rearrangement reactions), corrosion, and difficulty in the recovery of catalyst, especially the requirement of moisture-free solvents because these catalysts are moisture sensitive. Meanwhile, heterogeneous catalyst has a number of benefits such as the ease of separation and geometry selectivity. Therefore, the replacement of liquid acid catalysts in Friedel-Crafts reactions with heterogeneous catalysts is a promising strategy in green chemistry. Many types of solid catalysts have been studied such as Sb supporting K10 [1], Si-MCM-41-supported  $\text{Ga}_2\text{O}_3$  and  $\text{In}_2\text{O}_3$  [2], solid super acids based on sul-

fated  $\text{ZrO}_2$  [3],  $\text{Fe}(\text{OTf})_3$  [4], zinc-modified MCM-22 [5],  $\text{FeCl}_3$ ,  $\text{MnCl}_2$ ,  $\text{CoCl}_2$ ,  $\text{NiCl}_2$ ,  $\text{CuCl}_2$ ,  $\text{ZnCl}_2$  supported on acidic alumina [6], Hf/SBA-15 [7],  $\text{K}_2\text{FeZrP}_3\text{O}_{12}$  [8], FeY zeolite [9], mesoporous ALSBA-15 [10], ZSM-5 zeolites [11], silica-immobilized  $\text{FeCl}_3$  [12], H-Beta zeolite [13], mesoporous mordenite [14], niobium-containing zeolites [15], and ion-exchanged clays [16]. Cseri et al. [16] showed that the mechanism of benzylolation of benzene with benzyl chloride on solid catalysts differs from the classical acid mechanism. The reaction mechanism consisting of several redox stages has been proposed for the first time in the benzylolation of benzene and aromatic compounds with benzyl chloride and benzylic alcohol on different clay catalysts. Choudary et al. [17] studied the benzylolation of benzene, toluene, and other aromatic compounds on various metal-bentonite catalysts (pillared layered clay: PILC), FePILC, AlPILC, TiPILC, ZrPILC, and CePILC. The results showed that FePILC had the highest catalytic activity due to the

lower reduction potential of  $\text{Fe}^{3+}/\text{Fe}^{2+}$  pairs. In addition, the authors found that clay minerals containing only  $\text{Fe}^{3+}$  ions had weaker catalyst activity than clay with polycations or Fe oligomers did. Choudhary et al. [18] studied the benzylation and benzoylation reaction of aromatic compounds with benzyl chloride and benzoyl chloride on GaAlClx-Mont.K-10 catalyst. The high catalytic activity of GaAlClx-Mont.K-10 was due to the redox property of  $\text{Ga}^{3+}/\text{Ga}^+$ . The mechanism of the reaction included some redox stages as shown for Fe-, Zn-, Ga-, and In-modified ZSM-5 type zeolite catalysts [18, 19]. Bachari et al. [20] also clarified the redox mechanism in benzylation reaction of benzene and aromatic compounds on Fe-HMS-25 catalyst. It has been proposed earlier that the reaction could be initiated by an oxidation of benzyl chloride with the formation of a charge transfer complex.

Spinel ferrites are a class of magnetic materials that can be employed in several areas, such as magnetic devices, switching devices, catalysts, and adsorption [21, 22]. Zinc ferrite has long aroused researchers' attention owing to its unique magnetic properties including high magnetic permeability, nontoxicity, phase stability, and high electronic conductivity [23, 24] compared with other spinel ferrites. Zinc ferrite with multivalence states is expected as a good redox catalyst for the Friedel-Crafts reactions. According to our best knowledge, there are not many studies on the benzylation of *p*-xylene using zinc ferrite.

In the present paper, the kinetics of the adsorption of reactants on the catalyst surface and the kinetics and the mechanism of benzylation of *p*-xylene, as well as the relationship between adsorption kinetics and reaction kinetics of *p*-xylene benzylation over  $\text{ZnFe}_2\text{O}_4$  nanomaterial will be discussed.

## 2. Experimental

**2.1. Materials.** *p*-Xylene, isopropanol, ethylene glycol, and glycerol were purchased from Merck Company, and ferric nitrate nonahydrate ( $\text{Fe}(\text{NO}_3)_3 \cdot 9\text{H}_2\text{O}$ , 99.0%), zinc nitrate hexahydrate ( $\text{Zn}(\text{NO}_3)_2 \cdot 6\text{H}_2\text{O}$ , 99.0%), and sodium hydroxide (NaOH) were of analytical grade and were obtained from Guangzhou Company, China.

**2.2. Characterization.** The chemical composition of the samples was determined by EDX method using SEM-EDX Jeol 6490-JED 2300 (Japan) equipment. X-ray diffraction (XRD) patterns were recorded on D8 Advance Bruker, Germany, with  $\text{CuK}\alpha$  radiation ( $\lambda = 1.5406 \text{ \AA}$ ). The morphology of the product was characterized by scanning electron microscope (SEM, JMS-5300LV). Nitrogen adsorption-desorption isotherms were measured on Tri Star 3000. BET specific surface area was calculated from the nitrogen adsorption data with the relative pressure ranged from 0.04 to 0.25. Gas chromatography-mass spectrometry (GC-MS) method was used to qualitatively and quantitatively determine reaction products. The measurement was carried on Shimadzu, GC2010 software, detector: FID, bearing air flow rate of  $1.05 \text{ mL} \cdot \text{min}^{-1}$  at sample chamber temperature of  $1000^\circ\text{C}$  and sample volume of  $2 \mu\text{L}$ .

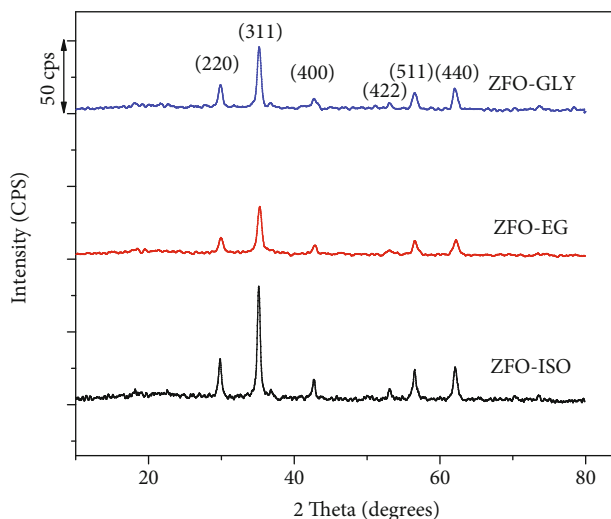


FIGURE 1: XRD patterns of ZFO-ISO, ZFO-EG, ZFO-GLY.

**2.3. Catalyst Preparation.** In a typical synthesis, 20 mL of solvent was added to 40 mL of distilled water. The mixture was then stirred with a magnetic stirrer at 750 rpm until the solvent was completely dissolved. Next, the solid mixture of  $\text{Zn}(\text{NO}_3)_2 \cdot 6\text{H}_2\text{O}$  and  $\text{Fe}(\text{NO}_3)_3 \cdot 9\text{H}_2\text{O}$  with molar ratio Fe:Zn of 2:1 was added into the mixed solvent under vigorously stirring at room temperature. 40 mL of 2 M NaOH solution was then added dropwise into this solution. The mixture was vigorously stirred for another 1 h, before being transferred into a teflon chamber which was placed in the stainless steel autoclave. The hydrothermal process was carried out at  $120^\circ\text{C}$  for 24 h. After the heating treatment, the autoclave was allowed to cool naturally to room temperature. The obtained black precipitate was filtered and washed several times with distilled water until pH reached 7.0. The obtained product was dried at  $80^\circ\text{C}$  and then calcined at  $500^\circ\text{C}$  for 4 h.

The spinel  $\text{ZnFe}_2\text{O}_4$  materials which were synthesized in isopropanol, ethylene glycol, and glycerol were denoted as ZFO-ISO, ZFO-EG, and ZFO-GLY, respectively.

**2.4. Catalytic Testing.** The alkylation reaction of *p*-xylene with benzyl chloride was carried out in a 250 mL two-neck flask with one being connected to the reflux condenser and the other one being sealed for use. The flask was mounted on a magnetic stirrer. 0.005 g of catalyst was added to the 2-neck flask, and then  $V_1$  mL of *p*-xylene was introduced. The temperature of the reaction system was adjusted to  $70^\circ\text{C}$ , and then  $V_2$  mL of benzyl chloride was injected to the flask. This time was considered as the zero time. After certain reaction times, samples were taken out and centrifuged to remove the catalyst. The conversion of benzyl chloride was determined from GC-MS results.

$$\text{Conversion}(\%) = \frac{S_o - S_t}{S_o} \cdot 100, \quad (1)$$

where  $S_o$  and  $S_t$  are the peak areas of benzyl chloride, respectively, at the zero time and at the time  $t$ .

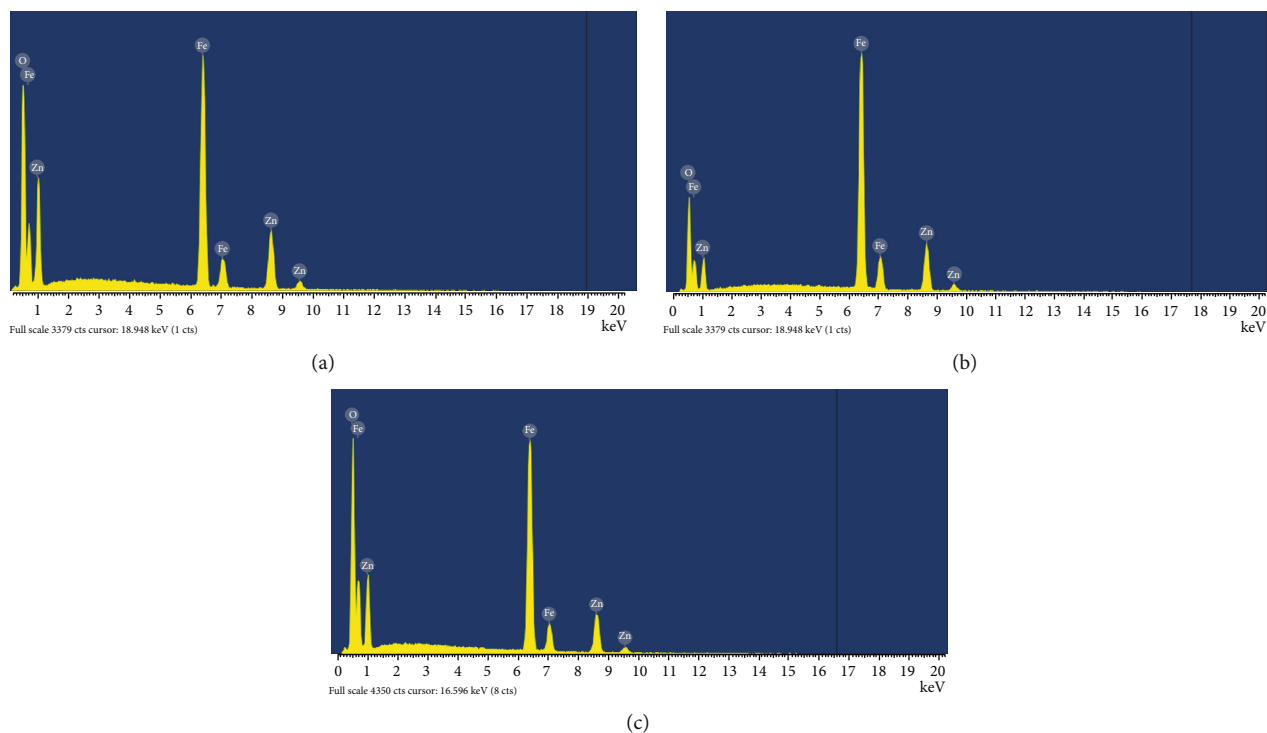


FIGURE 2: EDX analysis of (a) ZFO-ISO, (b) ZFO-EG, and (c) ZFO-GLY.

In kinetic experiments of *p*-xylene benzylation with benzyl chloride, the values of  $V_1$  and  $V_2$  were 23.9 mL and 1.1 mL, respectively (corresponding to *p*-xylene:benzylation molar ratio of 22:1). The reaction products and the conversion of benzyl chloride were determined by GC-MS method.

The influence of several factors to *p*-xylene benzylation with benzyl chloride was investigated by varying the molar ratio of *p*-xylene:benzyl chloride (22:1, 10:1, 6:1, and 3:1), the content of a catalyst (0.02 g, 0.01 g, and 0.005 g), and the reaction temperature (60°C, 65°C, 70°C, and 80°C).

**2.5. Adsorption of Benzyl Chloride and *p*-Xylene on ZFO-EG Catalyst.** The mixture of benzyl chloride and *p*-xylene with molar ratio of 1:1 was introduced into a 250-mL two-neck flask. The temperature of the solution was adjusted to 30°C, and then 0.5 g of ZFO-EG sample was added to the flask. The obtained mixture was stirred with a magnetic stirrer at a speed of 600 rpm for 2 hrs to attain equilibrium. At given time intervals, about 0.5 mL of solution was sampled out and centrifuged to remove the catalyst. Adsorption capacity of benzyl chloride and *p*-xylene was determined from GC-MS results.

### 3. Results and Discussion

**3.1. Characterization of the Catalysts.** Solvent has an effect on the dissolution of ions, which in turn affects the structural formation of the  $\text{ZnFe}_2\text{O}_4$  crystal. In order to investigate the influence of the solvent, the Fe/Zn molar ratio was fixed at 2: 1 with hydrothermal time of 24 hours, hydrother-

TABLE 1: Elemental composition of ZFO-ISO, ZFO-EG, and ZFO-GLY analyzed by EDX.

Sample	O	Fe	Zn	Fe/Zn ratio
ZFO-ISO	72.17	19.33	8.5	2.274
ZFO-EG	68.16	23.51	8.33	2.582
ZFO-GLY	73.06	20.32	6.62	3.069

mal temperature 120°C, calcination temperature of 500°C. Three solvents were chosen including isopropanol, ethylene glycol, glycerol. The XRD patterns of samples prepared in different solvents are shown in Figure 1.

The XRD patterns of all samples show peaks at  $2\theta$  values of 29.93°, 35.27°, 42.81°, 53.09°, 56.54°, and 62.19° which can be indexed to (220), (311), (400), (422), (333), and (440) crystal planes of  $\text{ZnFe}_2\text{O}_4$  crystal structure, respectively, according to ICD 22-1012 [21]. In addition, there is no diffraction peak of metal oxide residues such as ZnO and  $\text{Fe}_2\text{O}_3$  on XRD patterns, indicating that the obtained material was of high purity. The XRD patterns of ZFO-ISO shows sharp characteristic peaks with the strongest intensity, which means that this sample was in the best crystalline form. In contrast, the ZFO-EG sample showed the least ordered structure in three surveyed samples. The elemental characteristic of  $\text{ZnFe}_2\text{O}_4$  materials were studied by EDX method showing the existence of Zn, Fe, and O elements (Figure 2). Also, there is no evidence of remaining solvent in the samples.

The chemical composition of these three samples is summarized in Table 1.

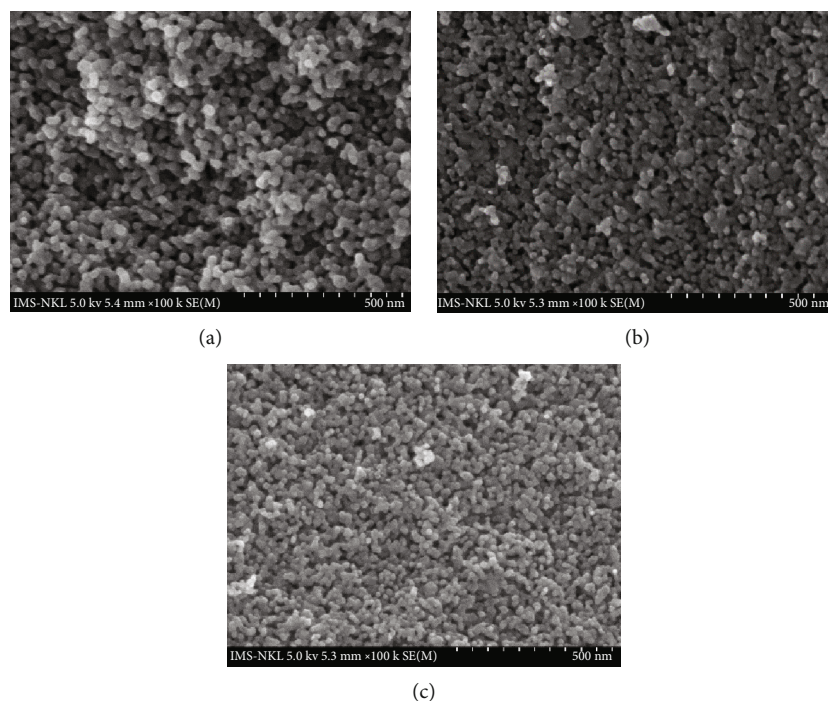


FIGURE 3: SEM images of (a) ZFO-ISO, (b) ZFO-EG, and (c) ZFO-GLY.

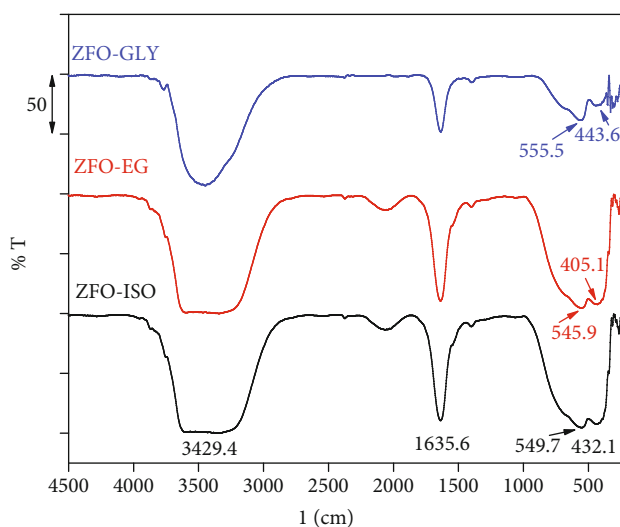


FIGURE 4: FTIR spectra of ZFO-ISO, ZFO-EG, and ZFO-GLY.

Experimentally, the molar ratio Fe/Zn was fixed at 2.0, while this ratio was found to be greater than 2 according to the EDX analysis, which shows that solvent affected the dispersion of  $\text{Fe}^{3+}$  and  $\text{Zn}^{2+}$  ions into the crystal lattice of  $\text{ZnFe}_2\text{O}_4$  material.

The surface morphology of the prepared samples was examined by SEM (Figure 3).

The morphology of  $\text{ZnFe}_2\text{O}_4$  samples synthesized in different solvents did not show significant difference. However, the particle size of the sample synthesized in isopropanol solvent was larger than that of the other two samples. The size of the particles observed from the SEM image ranged

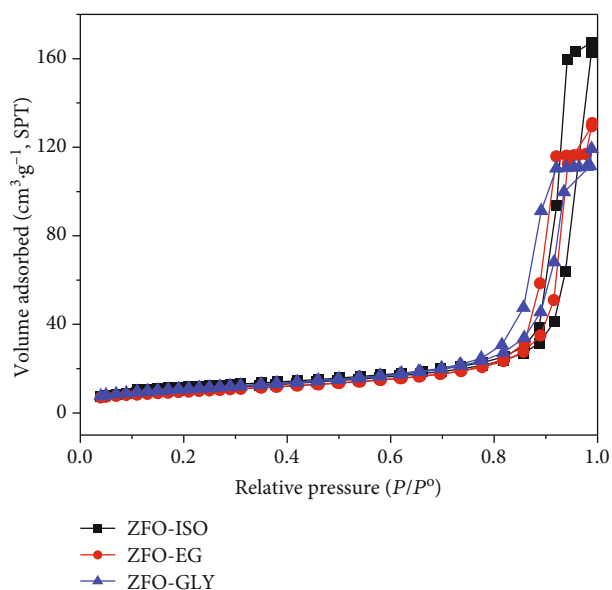


FIGURE 5:  $\text{N}_2$  adsorption/desorption isotherms of ZFO-ISO, ZFO-EG, and ZFO-GLY.

from 20 nm to 25 nm with agglomeration of nanoparticles which could be due to magnetic interactions between the particles.

FT-IR spectra of ZFO-ISO, ZFO-EG, and ZFO-GLY are presented in Figure 4. FT-IR spectra of all samples display a broad peak at  $3429.4\text{ cm}^{-1}$  corresponding to the stretching vibration of the adsorbed water molecules [21, 25, 26], a sharp peak at  $1635.6\text{ cm}^{-1}$  [21] attributed to the deformation band ( $\delta(\text{O-H})$ ). The characteristic peaks for Fe-O

TABLE 2: Textural parameters of ZFO-ISO, ZFO-EG, and ZFO-GLY samples.

Sample	$S_{BET}$ ( $m^2 \cdot g^{-1}$ )	$S_{mic}$ ( $m^2 \cdot g^{-1}$ )	$S_{ext}$ ( $m^2 \cdot g^{-1}$ )	$V_p$ ( $cm^3 \cdot g^{-1}$ )	$D_p$ (nm)
ZFO-ISO	37.17	5.48	31.69	0.25	23.38
ZFO-EG	34.34	4.04	30.30	0.18	18.15
ZFO-GLY	37.70	4.49	33.21	0.17	15.31

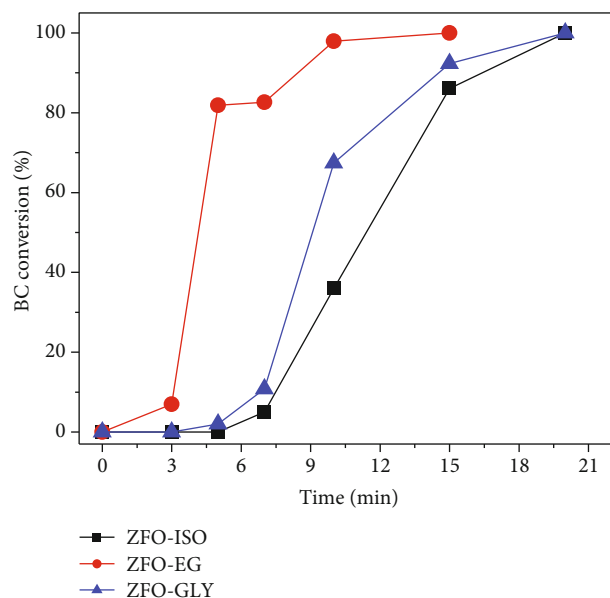


FIGURE 6: Benzyl chloride conversion vs. time over ZFO-ISO, ZFO-EG, and ZFO-GLY catalysts ( $T = 343$  K, molar ratio of  $p$ -xylene:benzyl chloride 22:1; catalytic mass: 0.005 g).

deformation vibration in ZFO-ISO, ZFO-EG, and ZFO-GLY samples are at  $432.1$ ,  $405.1$ , and  $443.6$   $cm^{-1}$ , respectively [27]. Peaks at  $549.7$   $cm^{-1}$  (ZFO-ISO),  $545.9$   $cm^{-1}$  (ZFO-EG), and  $555.5$   $cm^{-1}$  (ZFO-EG) correspond to Zn–O deformation vibration in tetrahedral site [21]. These interpretations indicate that the position of peaks relating to the interaction between oxygen and cations in tetrahedral and octahedral sites of  $ZnFe_2O_4$  structure depends on the used solvents.

The nitrogen adsorption-desorption isotherms of the samples are presented in Figure 5. According to the IUPAC classification, the isotherm curves of ZFO-ISO, ZFO-EG, and ZFO-GLY (Figure 5) are all type III. At relative pressure of  $p/p^0 = 0.8 - 1.0$ , the nitrogen adsorption and desorption isotherms of all samples exhibit hysteresis loop of type  $H3$  indicating the multilayer adsorption of  $N_2$  molecules onto the pores of material (these pores could be related to the arrangement of adjacent nanoparticles of material). The textural properties of all the samples are listed in Table 2.

Table 2 shows that  $S_{BET}$  of ZFO-ISO, ZFO-EG, and ZFO-GLY were found to be  $37.17$ ,  $34.34$ , and  $37.70$   $m^2 \cdot g^{-1}$ , respectively. The BET surface areas are mainly due to the contribution of external areas. The pore width of ZFO-ISO, ZFO-EG, and ZFO-GLY materials determined by Barrett–Joyner–Halenda (BJH) method are  $23.38$ ,  $18.15$ , and  $15.31$  nm, respectively, which corresponds to the arrange-

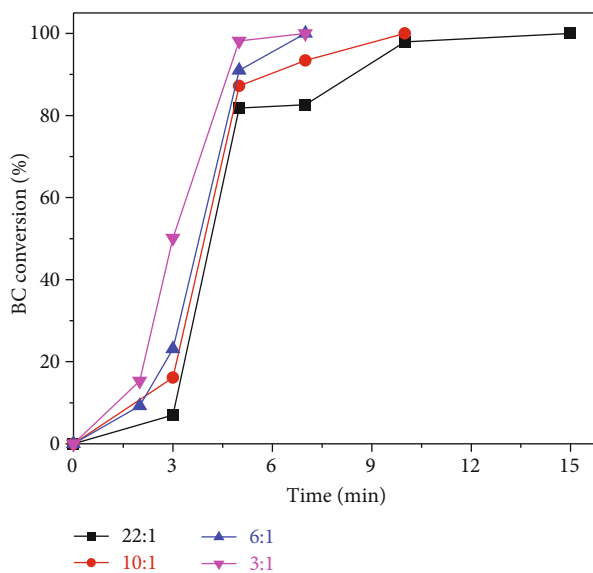


FIGURE 7: Influence of molar ratios of  $p$ -xylene and benzyl chloride on the conversion of benzyl chloride over the ZFO-EG catalyst ( $T = 343$  K; catalyst mass: 0.005 g).

ment of the  $ZnFe_2O_4$  nanoparticles. The relatively large surface area of all samples was expected to provide many active catalytic sites for the  $p$ -xylene benzylation.

**3.2. Comparison of Catalysts for  $p$ -Xylene Benzylation.** In this section, the synthesized  $ZnFe_2O_4$  materials were used as catalysts for the  $p$ -xylene benzylation. Figure 6 shows the conversion of benzyl chloride (BC) versus time in  $p$ -xylene benzylation over ZFO-ISO, ZFO-EG, and ZFO-GLY catalysts.

The results show that the BC conversion reached 100% after 15 minutes over ZFO-EG catalyst and 20 minutes over ZFO-ISO and ZFO-GLY catalysts. The product 2,5-Dimethyldiphenylmethane (2,5-DMDPM) appeared in 3 minutes over the ZFO-EG catalyst and in 5 minutes and 7 minutes over the ZFO-GLY and ZFO-ISO samples, respectively. In the same time of reaction, the highest BC conversion was found with the use of ZFO-EG catalyst, followed by the ZFO-EG and ZFO-ISO catalysts. It is interesting that the ZFO-ISO sample which had a large surface area and the best crystallinity of all the investigated samples showed the lowest BC conversion. Meanwhile, the ZFO-EG sample with the lowest surface area and the least crystallinity provided the highest BC conversion in the same reaction time. This demonstrates that the catalytic activity of  $ZnFe_2O_4$  does not depend much on the structural nature of the material.

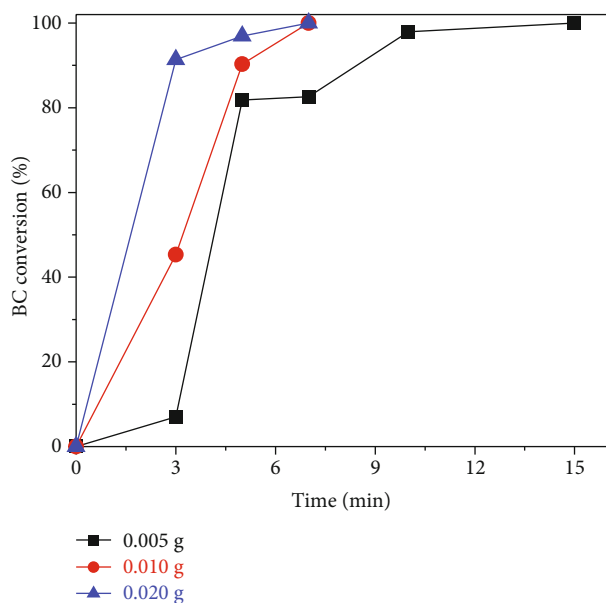


FIGURE 8: Influence of catalyst amount on the percentage conversion of benzyl chloride over ZFO-EG catalyst ( $T = 343$  K, molar ratio of *p*-xylene:benzyl chloride = 22:1).

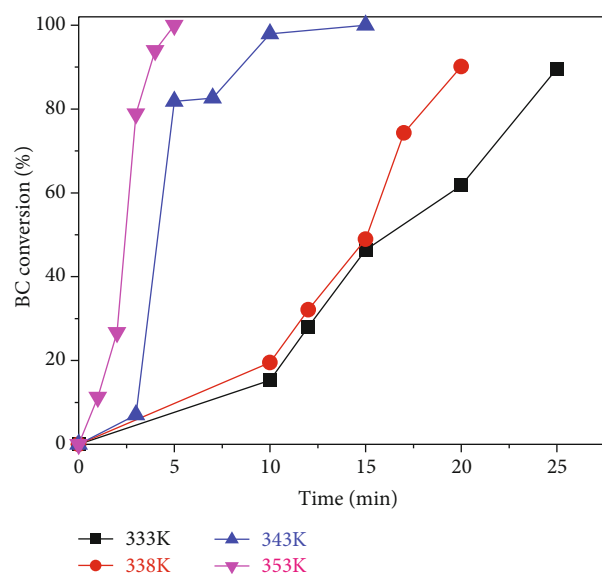


FIGURE 9: The conversion of benzyl chloride vs. time over ZFO-EG catalyst at different temperatures (molar ratio of *p*-xylene:benzyl chloride 22:1, catalytic mass 0.005 g).

In addition, it was found that although the surface area of ZFO-ISO and ZFO-GLY samples was similar ( $\approx 37 \text{ m}^2 \cdot \text{g}^{-1}$ ), their catalytic activity was different. According to EDX data, the Fe content in the synthesized samples decreased gradually in the order of ZFO-EG, ZFO-GLY, and ZFO-ISO. Since the number of Fe sites was related to the catalytic activity for *p*-xylene benzylation, the Fe content in the material was proposed to be responsible for the best catalytic activity of the ZFO-EG sample [28]. This is similar with the report of Choudary et al. [19] in the toluene benzylation reaction.

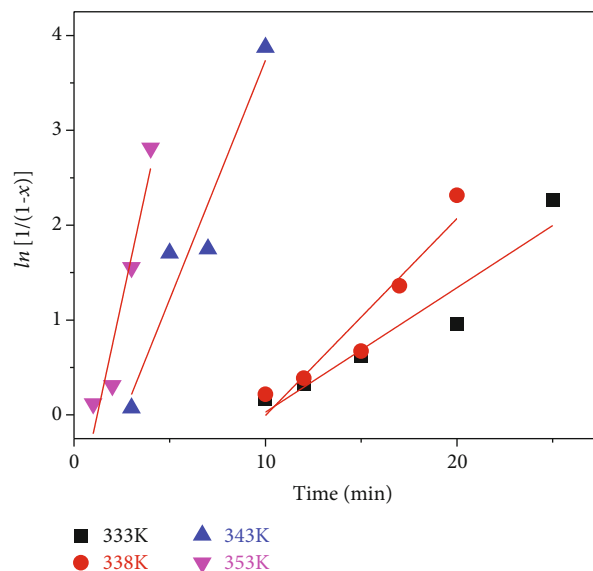


FIGURE 10: Plot of first order kinetic model of *p*-xylene benzylation over ZFO-EG catalyst at different temperatures.

TABLE 3: The parameters of the *pseudo*-first-order kinetic model for *p*-xylene benzylation over ZFO-EG catalyst.

Temperature (K)	$k$ ( $\text{min}^{-1}$ )	$R^2$
333	0.131	0.914
338	0.208	0.916
343	0.503	0.931
353	0.933	0.928

Furthermore, the reaction products contained only 2,5-DMDPM without any by-products. Normally, the alkylation reaction is difficult to stop at a single alkylation because the alkyl group is an electron-donating group that can attack many positions on the aromatic ring, leading to multiple alkylation. To avoid multialkylation, an excess amount of aromatic compounds is recommended. However, the study of Sebti et al. [21] demonstrated that dialkyl products also occurred in the alkylation using HAP,  $\text{ZnCl}_2/\text{HAP}$ ,  $\text{NiCl}_2/\text{HAP}$ , and  $\text{CuCl}_2/\text{HAP}$  catalysts in spite of the excess of aromatic compounds. Furthermore, recent publications [29–31] indicated that benzylation of aromatic compounds was often accompanied by side products. To verify this result, the reaction time was extended to 1 h. However, the GC-MS chromatogram did not show any side products. From this study, the ZFO-EG sample was selected for further investigation.

### 3.3. Factors That Affect *P*-Xylene Benzylation

**3.3.1. Effect of Molar Ratio of Reactants.** Figure 7 shows the benzyl chloride percentage conversion vs. reaction time over the ZFO-EG catalyst at different molar ratios of *p*-xylene and benzyl chloride. The reaction product was only mono-benzylated product. The percentage conversion of benzyl chloride was found to increase as the molar ratio of *p*-xylene:benzyl chloride decreased from 22:1 to 3:1. At the molar

TABLE 4: A comparison of some reaction parameters of the present catalyst with previous works.

Catalyst	Molar ratio <i>p</i> -xylene:benzyl chloride	Catalytic mass (g)	Temp. (K)	$k'$ ( $\text{g}^{-1}\cdot\text{min}^{-1}$ )	$k$ ( $\text{min}^{-1}$ )	Ref
Fe-HMS-50	15:1	0.1	343	0.275	0.026	[20]
Cu-HMS-50	15:1	0.1	343	0.183	0.018	[30]
FAPO4-5	15:1	0.1	343	0.447	0.048	[32]
ZFO-EG	22:1	0.005	343	100.6	0.503	The present work

ratio of 22:1, the percentage conversion of benzyl chloride increased slightly at 3 minutes, then the percentage conversion grew rapidly from 3 to 10 minutes, and the reaction time required for complete conversion of BC was 15 minutes. Meanwhile, with a molar ratio of 6:1 and 3:1, the percentage conversion reached 100% after only 7 minutes.

This result suggests that the percentage conversion of benzyl chloride strongly depends on the molar ratio of the reactants. The greater the molar ratio of *p*-xylene/benzyl chloride is, the lower the percentage conversion of benzyl chloride is. This can be due to the inefficient contact between the reactants and catalytic sites. However, to study the reaction dynamics in the next sections, the molar ratio of *p*-xylene:benzyl chloride of 22:1 was chosen. The concentration of *p*-xylene at this molar ratio was greater than benzyl chloride, so the reaction rate was considered to depend only upon the concentration of benzyl chloride.

**3.3.2. Effect of Catalyst Amount.** In heterogeneous catalyst reaction, the amount of catalyst plays an important role. As the amount of catalyst increases, the number of catalytic sites increases, which can directly affects the reaction rate. In this study, the mass of the catalyst was varied from 0.020 to 0.005 g. The dependence of benzyl chloride percentage conversion vs. reaction time is presented in Figure 8.

As shown in Figure 8, the percentage conversion of benzyl chloride increased with the catalyst amount with the product being solely monoalkyl-substituted benzene. The availability of more catalytic sites boosted the interaction with the reactants leading to higher percentage conversion of benzyl chloride.

**3.3.3. The Effect of Reaction Temperature.** Figure 9 shows the percentage conversion of benzyl chloride vs. time over the ZFO-EG catalyst at different temperatures.

From Figure 9, it can be seen that the conversion of benzyl chloride increased when increasing reaction temperature from 333 to 353 K. Again only 2,5-DMDPM was obtained as the final product without any dialkyl products being detected. The reaction time required to convert 100% of benzyl chloride was 5 minutes at 353 K.

At a given temperature and with an excess amount of *p*-xylene, experimental data obtained were correlated with the *pseudo*-first order kinetic model [32].

$$\ln\left(\frac{1}{1-x}\right) = k.t, \quad (2)$$

where  $x$  is the conversion of benzyl chloride,  $t$  is the reaction time (minutes), respectively, and  $k$  is *pseudo*-rate constant ( $\text{min}^{-1}$ ).

The slope of the linear plot of  $\ln(1/(1-x))$  vs. time  $t$  provides the value of  $k$ .

The linear plot of first-order kinetic model at different temperatures is illustrated in Figure 10.

The parameters obtained from the first-order kinetic equation are summarized in Table 3.

From Table 3, it is found that the rate constant of *p*-xylene benzylation over ZFO-EG catalyst is high and the reaction rate increases with temperature in the order of 333 K ( $k = 0.131 \text{ min}^{-1}$ ) > 338 K ( $k = 0.208 \text{ min}^{-1}$ ) > 343 K ( $k = 0.503 \text{ min}^{-1}$ ) > 353 K ( $k = 0.933 \text{ min}^{-1}$ ). A comparison of the catalytic activity in this present work with those reported previously is listed in Table 4. As seen from the table, despite a considerably small (0.005 g) amount of catalyst used in the present work, rate constant  $k$  of this *p*-xylene benzylation over ZFO-EG is about 366, 550, and 211 times higher than over Fe-HMS-50, Cu-HMS-50, and FAPO4-5 catalysts reported by Bachari [20, 30, 32] (of  $0.275 \text{ g}^{-1}\cdot\text{min}^{-1}$  ( $k = 0.0275 \text{ min}^{-1}$ ),  $0.183 \text{ g}^{-1}\cdot\text{min}^{-1}$  ( $k = 0.0183 \text{ min}^{-1}$ ), and  $0.447 \text{ g}^{-1}\cdot\text{min}^{-1}$  ( $k = 0.0477 \text{ min}^{-1}$ ), respectively). This demonstrates the high catalytic activity of ZFO-EG catalyst in *p*-xylene benzylation.

The activation energy of the reaction can be calculated by using the Arrhenius equation as follows:

$$\ln k = -\frac{E_a}{RT} + \ln A, \quad (3)$$

where  $E_a$  is the activation energy,  $k$  the rate constant, and  $A$  the frequency factor.

From Figure 11, the activation energy of *p*-xylene benzylation on the ZFO-EG catalyst was determined to be  $98.9 \text{ kJ}\cdot\text{mol}^{-1}$ . The activation energy of benzylation of benzene reactions reported by Lin et al. [33] was high,  $132.6 \text{ kJ}\cdot\text{mol}^{-1}$  over 8-FeZ catalyst and  $140.2 \text{ kJ}\cdot\text{mol}^{-1}$  over 2.5-FeZ catalyst. This indicates that the activation energy of *p*-xylene benzylation over ZFO-EG catalyst was smaller than that of the benzene benzylation reported by Lin et al. [33].

### 3.3.4. Leaching Experiment and Catalytic Reusability

**(1) Leaching Experiment.** In order to prove that ZFO-EG was a heterogeneous catalyst in alkylation reaction, an experiment was run in the conditions: molar ratio of *p*-xylene : benzyl chloride = 22 : 1, the reaction temperature 338 K, and mass of catalyst 0.005 g. After 14 minutes, the reaction mixture was hot-filtered to separate the catalyst solid, and

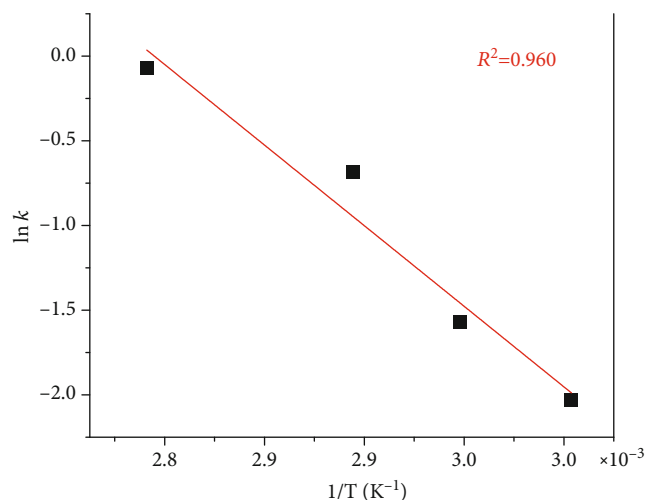


FIGURE 11: The plot of  $\ln k$  versus  $1/T$  of *p*-xylene benzylation over ZFO-EG catalyst.

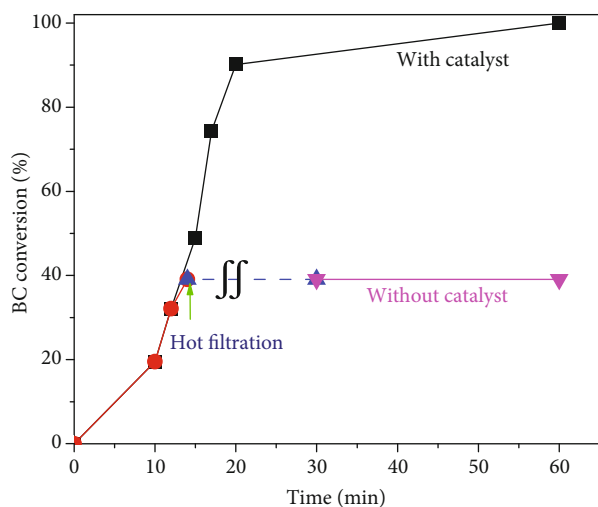


FIGURE 12: The leaching experiment for ZFO-EG catalyst of benzylation reaction.

then the reaction was further processed at 338 K with the absence of catalyst (Figure 12). After 60 minutes, the percentage conversion was almost unchanged. This confirmed that ZFO-EG acted as a heterogeneous catalyst in this reaction.

(2) *Catalytic Reusability*. The recovery of the catalyst is critical for catalyst application in terms of cost and environmental pollution. In this study, the ZFO-EG catalyst for the first use was recovered, washed several times with ethanol, dried at 373 K for 24 h, and then used as a catalyst for *p*-xylene benzylation for the second experiment. The catalyst recovery in the second use was conducted similarly. Figure 13 represents the catalytic reusability.

The results show that the percentage conversion of benzyl chloride over ZFO-EG catalyst slightly decreased in three successive uses. After 15 minutes of reaction, the percentage

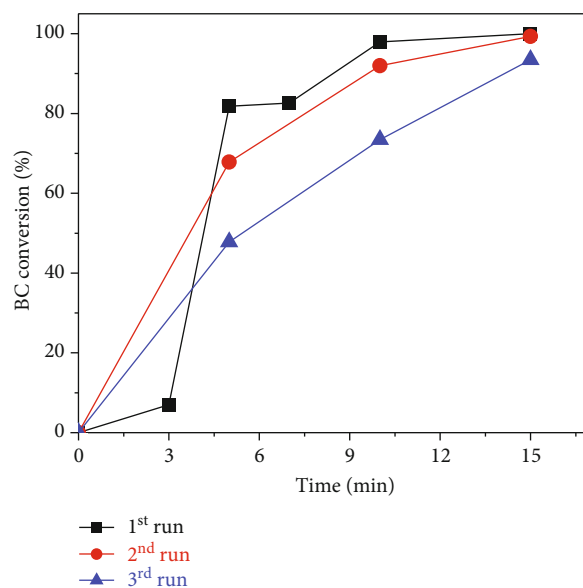


FIGURE 13: The conversion of benzyl chloride over time on the original ZFO-EG catalyst and reuse (molar ratio of *p*-xylene:benzyl chloride 22:1, catalyst mass 0.005 g, and temperature 343 K).

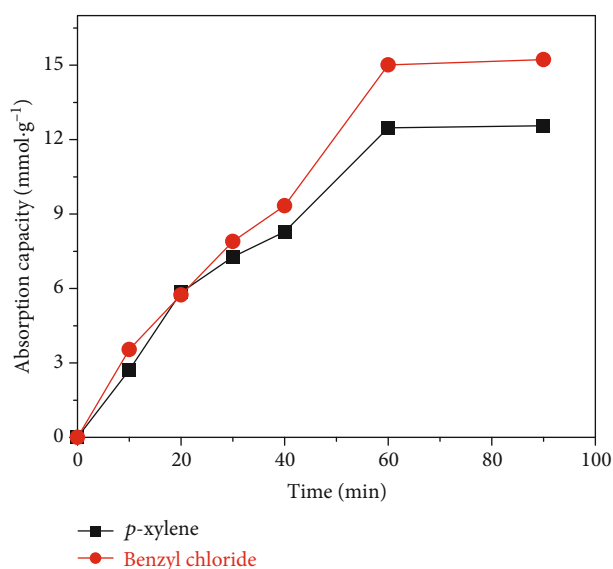


FIGURE 14: Absorption capacity of benzyl chloride and *p*-xylene versus time over ZFO-EG catalyst (molar ratio of *p*-xylene:benzyl chloride 1:1, catalytic mass 0.5 g, and temperature 303 K).

conversion for the first use reached 99.3%, while the value of conversion for the second use was 93.5%. These results imply that the catalyst could be reused for several times.

### 3.4. Kinetics of *p*-Xylene Benzylation over ZFO-EG Catalyst

3.4.1. *Adsorption of Benzyl Chloride and P-Xylene over ZFO-EG Catalyst*. The adsorption capacity of benzyl chloride and *p*-xylene at the molar ratio of 1:1 over the ZFO-EG catalyst ( $m = 0.5$  g) at the temperature of 303 K is shown in Figure 14. It can be seen that there was a simultaneous adsorption of

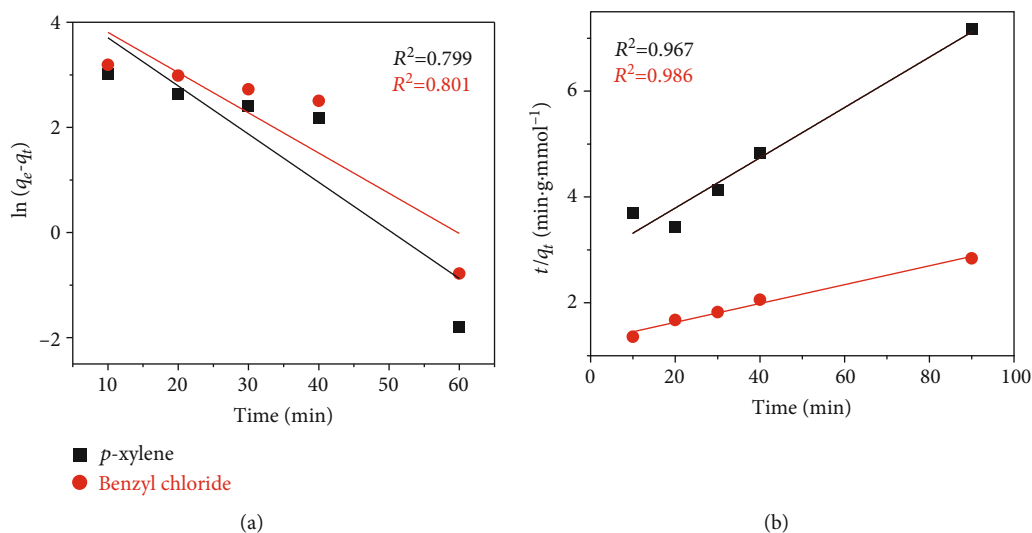
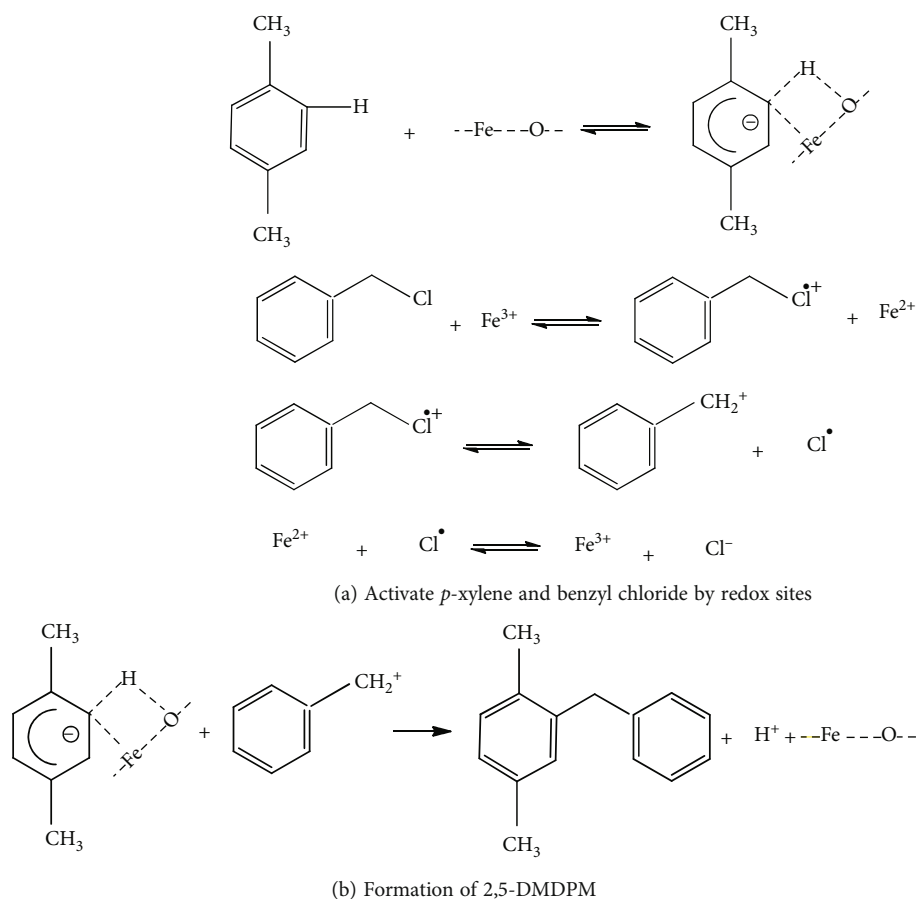


FIGURE 15: The *pseudo*-first-order kinetic model (a) and *pseudo*-second-order kinetic model (b) of benzyl chloride and *p*-xylene adsorption by ZFO-EG catalyst.



SCHEME 1: *p*-Xylene benzylation mechanism over ZFO-EG catalyst.

benzyl chloride and *p*-xylene over ZFO-EG catalyst with adsorption capacity decreasing in the order benzyl chloride > *p*-xylene. Therefore, the adsorption of *p*-xylene could follow the Langmuir–Hinshelwood mechanism.

(1) *Adsorption Kinetics*. In order to investigate the adsorption kinetics of benzyl chloride and *p*-xylene over ZFO-EG catalyst, the *pseudo*-first-order and *pseudo*-second-order kinetic models were applied.

The *pseudo*-first-order model is given by

$$\ln (q_e - q_t) = \ln q_e - k_1 \cdot t, \quad (4)$$

where  $q_e$  and  $q_t$  ( $\text{mmol.g}^{-1}$ ) are the uptake of adsorbent (*p*-xylene or benzyl chloride) at equilibrium and at time  $t$  and  $k_1$  is the first order rate constant ( $\text{min}^{-1}$ ).

The adsorption uptake of *p*-xylene or benzyl chloride by the adsorbent was calculated by

$$q_t = \frac{C_o - C_t}{m} \cdot V, \quad (5)$$

where  $q_t$  is the adsorption uptake of *p*-xylene or benzyl chloride on the adsorbent at time  $t$ ,  $C_o$  and  $C_t$  ( $\text{mol.L}^{-1}$ ) are *p*-xylene or benzyl chloride concentration at initial and a certain time,  $t$ , respectively,  $V$  (L) is the volume of phenol red solution, and  $m$  (g) is the mass of the adsorbent [34, 35].

The *pseudo*-second-order kinetic model is given by

$$\frac{t}{q_t} = \frac{1}{k_2 q_e^2} + \frac{1}{q_e} \cdot t, \quad (6)$$

where  $k_2$  is the rate constant of *pseudo*-second-order kinetic model ( $\text{g.mmol}^{-1}.\text{min}^{-1}$ ) [36].

The *pseudo*-first-order and *pseudo*-second-order kinetic models of adsorption of benzyl chloride and *p*-xylene by ZFO-EG catalyst are illustrated in Figure 15.

The high coefficients ( $R^2 > 0.967$ ) indicated that *pseudo*-second-order kinetic model was more suitable to illustrate the benzyl chloride and *p*-xylene adsorption on ZFO-EG catalyst. Experimental data showed that the *p*-xylene adsorption rate ( $k_2 = 7.94 \times 10^{-4} \text{ g.mmol}^{-1}.\text{min}^{-1}$ ) was three times faster than benzyl chloride adsorption rate ( $k_2 = 2.48 \times 10^{-4} \text{ g.mmol}^{-1}.\text{min}^{-1}$ ). From the analysis of adsorption kinetics, it was found that the adsorption of benzyl chloride and *p*-xylene by ZFO-EG catalyst could be chemisorption. Studies on benzylation of *p*-xylene or benzylation of benzene over FAPO<sub>4</sub>-5 [31] and FeKIT-5 [37] both indicated that the Fe<sup>3+</sup>/Fe<sup>2+</sup> redox sites might activate benzyl chloride and *p*-xylene (or benzene). In this study, the adsorption rate of benzyl chloride and *p*-xylene were fast and without any competition. Therefore, it can be proposed that *p*-xylene might first adsorb on the surface of the catalyst to form activated complexes. These complexes then interacted with the C<sub>6</sub>H<sub>5</sub>-CH<sub>2</sub><sup>+</sup> carbocation formed during the adsorption of benzyl chloride onto catalyst to give the products. Thus, the reaction kinetic could be described by Langmuir-Hinshelwood model. When an excess amount of *p*-xylene was used, this model became the first-order kinetic model as mentioned above.

**3.4.2. Proposed Reaction Mechanism.** Bachari et al. [30] and Hentit et al. [31] reported that the mechanism of benzylation of aromatic compounds over solid catalysts containing Fe sites involved a redox step at the reaction initiation. Based on the obtained experimental results and the mechanism for the benzylation proposed earlier, the mechanism of

*p*-xylene benzylation over ZFO-EG catalyst are proposed as follows (Scheme 1):

This reaction mechanism illustrates the Langmuir-Hinshelwood kinetics model, in which both *p*-xylene and benzyl chloride are chemically adsorbed on the redox sites of Fe.

## 4. Conclusion

ZFO-EG material exhibited an excellent catalytic activity for *p*-xylene benzylation with high conversion. The rate of *p*-xylene benzylation increased with increasing molar ratio of reactants, catalyst mass, and temperature. Activation energy of *p*-xylene benzylation over Fe-bentonite catalyst was found to be 98.9 kJ.mol<sup>-1</sup>. The Langmuir-Hinshelwood mechanism was suitable to describe the kinetics of *p*-xylene benzylation over solid ZFO-EG catalyst. The ZFO-EG can be regenerated and used effectively after three uses for catalyzing *p*-xylene benzylation.

## Data Availability

The data used to support the findings of this study are available from the corresponding author upon request.

## Conflicts of Interest

The authors declare that they have no conflicts of interest.

## Acknowledgments

This work was supported by Hue University under Decision DHH2021-03-161.

## References

- [1] A. B. Deshpande, A. R. Bajpai, and S. D. Samant, "The enhanced activity of Sb after supporting on K10 in the benzylation of benzene using benzyl chloride and benzyl alcohol," *Applied Catalysis A: General*, vol. 209, no. 1-2, pp. 229-235, 2001.
- [2] V. R. Choudhary, S. K. Jana, and B. P. Kiran, "Highly active Si-MCM-41-supported Ga<sub>2</sub>O<sub>3</sub> and In<sub>2</sub>O<sub>3</sub> catalysts for friedel-crafts-type benzylation and acylation reactions in the presence or absence of moisture," *Journal of Catalysis*, vol. 192, no. 2, pp. 257-261, 2000.
- [3] S. N. Koyande, R. G. Jaiswal, and R. V. Jayaram, "Reaction kinetics of benzylation of benzene with benzyl chloride on sulfate-treated metal oxide catalysts," *Industrial & Engineering Chemistry Research*, vol. 37, no. 3, pp. 908-913, 1998.
- [4] A. Bhattacharya, P. M. Shukla, and B. Maji, "Fe (OTf)<sub>3</sub>-catalysed Friedel-Crafts reaction of benzenoid arenes with  $\alpha,\beta$ -unsaturated carbonyl compounds: easy access to 1,1-diaryllalkanes," *Royal Society Open Science*, vol. 4, no. 10, article 170748, 2017.
- [5] S. V. Lande, A. Sakthivel, K. V. V. S. B. S. R. Murthy, U. Sreedharan, J. Das, and R. V. Jasra, "Zinc-modified MCM-22 as potential solid acid catalyst for Friedel-Crafts alkylation reaction," *International Journal of Chemical Reactor Engineering*, vol. 11, no. 1, pp. 407-415, 2013.

- [6] M. Salavati-Niasari, J. Hasanalian, and H. Najafian, "Alumina-supported  $\text{FeCl}_3$ ,  $\text{MnCl}_2$ ,  $\text{CoCl}_2$ ,  $\text{NiCl}_2$ ,  $\text{CuCl}_2$ , and  $\text{ZnCl}_2$  as catalysts for the benzylation of benzene by benzyl chloride," *Journal of Molecular Catalysis A: Chemical*, vol. 209, no. 1-2, pp. 209–214, 2004.
- [7] Y.-B. Huang, Y.-J. Luo, and F. Wang, "Hafnium-doped mesoporous silica as efficient Lewis acidic catalyst for Friedel–Crafts alkylation reactions," *Nanomaterials*, vol. 9, no. 8, p. 1128, 2019.
- [8] N. Sheikhana and A. R. Hajipourb, " $\text{K}_2\text{FeZrP}_3\text{O}_{12}$  as an efficient catalyst for Friedel–Crafts benzylation under solvent-free conditions," *Acta Chemica Iasi*, vol. 24, no. 2, pp. 102–111, 2016.
- [9] A. M. F. Bidart, A. P. S. Borges, H. C. Chagas, L. Nogueira, E. R. Lachter, and C. J. A. Mota, "Mechanistic aspects of Friedel–Crafts alkylation over FeY zeolite," *Journal of the Brazilian Chemical Society*, vol. 17, no. 4, pp. 758–762, 2006.
- [10] A. Vinu, D. P. Sawant, K. Ariga, M. Hartmann, and S. B. Halilgudi, "Benzylation of benzene and other aromatics by benzyl chloride over mesoporous AlSBA-15 catalysts," *Microporous Materials*, vol. 80, no. 1-3, pp. 195–203, 2005.
- [11] Y. Wang, J. Song, N. C. Baxter, G.-T. Kuo, and S. Wang, "Synthesis of hierarchical ZSM-5 zeolites by solid-state crystallization and their catalytic properties," *Journal of Catalysis*, vol. 349, pp. 53–65, 2017.
- [12] X. Pu and Y. Su, "Heterogeneous catalysis in microreactors with nanofluids for fine chemicals syntheses: benzylation of toluene with benzyl chloride over silica-immobilized  $\text{FeCl}_3$  catalyst," *Chemical Engineering Science*, vol. 184, pp. 200–208, 2018.
- [13] Z. Wang, L. Wang, Z. Zhou et al., "Benzylation of arenes with benzyl chloride over H-Beta zeolite: effects from acidity and shape-selectivity," *The Journal of Physical Chemistry*, vol. 121, pp. 15248–15255, 2017.
- [14] S. K. Saxena and N. Viswanadham, "Enhanced catalytic properties of mesoporous mordenite for benzylation of benzene with benzyl alcohol," *Applied Surface Science*, vol. 392, pp. 384–390, 2017.
- [15] A. Feliczak-Guzik, M. Sprynskyy, I. Nowak, M. Jaroniec, and B. Buszewski, "Application of novel hierarchical niobium-containing zeolites for synthesis of alkyl lactate and lactic acid," *Journal of Colloid and Interface Science*, vol. 516, pp. 379–383, 2018.
- [16] T. Cseri, S. Békássy, F. Figueras, and S. Rizner, "Benzylation of aromatics on ion-exchanged clays," *Journal of Molecular Catalysis A: Chemical*, vol. 98, no. 2, pp. 101–107, 1995.
- [17] B. M. Choudary, M. L. Kantam, M. Sateesh, K. K. Rao, and P. L. Santhi, "Iron pillared clays – efficient catalysts for Friedel–Crafts reactions," *Applied Catalysis A: General*, vol. 149, no. 1, pp. 257–264, 1997.
- [18] V. R. Choudhary and R. Jha, " $\text{GaAlCl}_{x-x}$ -grafted Mont.K-10 clay: highly active and stable solid catalyst for the Friedel–Crafts type benzylation and acylation reactions," *Catalysis Communications*, vol. 9, no. 6, pp. 1101–1105, 2008.
- [19] V. R. Choudhary and S. K. Jana, "Benzylation of benzene by benzyl chloride over Fe-, Zn-, Ga- and in-modified ZSM-5 type zeolite catalysts," *Applied Catalysis A: General*, vol. 224, no. 1-2, pp. 51–62, 2002.
- [20] K. Bachari, J. M. M. Millet, B. Cherifi, and O. Cherifi, "Benzylation of benzene by benzyl chloride over iron mesoporous molecular sieves materials," *Journal of Catalysis*, vol. 221, no. 1, pp. 55–61, 2004.
- [21] N. M. Mahmoodi, J. Abdi, and D. Bastani, "Direct dyes removal using modified magnetic ferrite nanoparticle," *Journal of Environmental Health Science and Engineering*, vol. 12, no. 1, 2014.
- [22] R. C. De Oliveira, R. P. Ribeiro, G. H. Cruvinel et al., "Role of surfaces in the magnetic and ozone gas-sensing properties of  $\text{ZnFe}_2\text{O}_4$  Nanoparticles: theoretical and experimental insights," *ACS Applied Materials & Interfaces*, vol. 13, no. 3, pp. 4605–4617, 2021.
- [23] T. R. Tatarchuk, N. D. Paliychuk, M. Bououdina et al., "Effect of cobalt substitution on structural, elastic, magnetic and optical properties of zinc ferrite nanoparticles," *Journal of Alloys and Compounds*, vol. 731, pp. 1256–1266, 2018.
- [24] T. R. Aisida, S. O. Ahmad, and I. Ezema, "Effect of calcination on the microstructural and magnetic properties of Pva, Pvp and Peg assisted zinc ferrite nanoparticles," *Physica B: Condensed Matter*, vol. 579, article 411907, 2020.
- [25] A. Ranjbaran, F. Abbasi, M. Khazaei, and A. R. Moosavi-Zareb, "Synthesis, characterization and application of  $\text{ZnFe}_2\text{O}_4$  nanoparticles as a heterogeneous ditopic catalyst for the synthesis of pyrano[2,3-d] pyrimidines," *RSC Advances*, vol. 5, no. 18, pp. 13643–13647, 2015.
- [26] S. Kashefi, S. M. Borghei, and N. M. Mahmoodi, "Covalently immobilized laccase onto graphene oxide nanosheets: preparation, characterization, and biodegradation of azo dyes in colored wastewater," *Journal of Molecular Liquids*, vol. 276, pp. 153–162, 2019.
- [27] J. Abdi, N. Mo, M. Mahmoodi, and I. A. Vossoughi, "Synthesis of magnetic metal-organic framework nanocomposite ( $[\text{email protected}]_2\text{@MnFe}_2\text{O}_4$ ) as a novel adsorbent for selective dye removal from multicomponent systems," *Microporous and Mesoporous Materials*, vol. 273, pp. 177–188, 2019.
- [28] H. Duraka and S. Genel, "Catalytic hydrothermal liquefaction of *Lactuca scariola* with a heterogeneous catalyst: the investigation of temperature, reaction time and synergistic effect of catalysts," *Bioresource Technology*, vol. 309, 2020.
- [29] A. E. Ahmed and F. Adam, "The benzylation of benzene using aluminium, gallium and iron incorporated silica from rice husk ash," *Microporous and Mesoporous Materials*, vol. 118, no. 1-3, pp. 35–43, 2009.
- [30] K. Bachari and O. Cherifi, "Benzylation of benzene and other aromatics by benzyl chloride over copper- mesoporous molecular sieves materials," *Catalysis Communications*, vol. 7, no. 12, pp. 926–930, 2006.
- [31] H. Hentit, K. Bachari, M. S. Ouali, M. Womes, B. Benaichouba, and J. C. Jumas, "Alkylation of benzene and other aromatics by benzyl chloride over iron- containing aluminophosphate molecular sieves," *Journal of Molecular Catalysis A: Chemical*, vol. 275, no. 1-2, pp. 158–166, 2007.
- [32] N. M. Mahmoodi, "Binary catalyst system dye degradation using photocatalysis," *Fibers and Polymers*, vol. 15, no. 2, pp. 273–280, 2014.
- [33] T. Lin, X. Lang, R. Li, T. Bai, and S. Yang, "Synergistic catalysts of isolated  $\text{Fe}^{3+}$  and  $\text{Fe}_2\text{O}_3$  on  $\text{FeO}_x/\text{HZSM-5}$  catalysts for Friedel–Crafts benzylation of benzen," *Chinese Chemical Letters*, vol. 22, no. 6, pp. 639–642, 2011.
- [34] N. M. Mahmoodi and M. H. Saffar-Dastgerdi, "Zeolite nanoparticle as a superior adsorbent with high capacity: synthesis, surface modification and pollutant adsorption ability from wastewater," *Microchemical Journal*, vol. 145, pp. 74–83, 2019.

- [35] J. Abdi, M. Vossoughi, N. M. Mahmoodi, and I. Alemzadeh, "Synthesis of amine-modified zeolitic imidazolate framework-8, ultrasound- assisted dye removal and modeling," *Ultrasonics Sonochemistry*, vol. 39, pp. 550–564, 2017.
- [36] N. M. Mahmoodi, M. Taghizadeh, A. Taghizadeh, J. Abdi, B. Hayati, and A. A. Shekarchi, "Bio-based magnetic metal-organic framework nanocomposite: ultrasound-assisted synthesis and pollutant (heavy metal and dye) removal from aqueous media," *Applied Surface Science*, vol. 480, pp. 288–299, 2019.
- [37] C. Anand, S. V. Priya, G. Lawrence et al., "Cage type mesoporous ferrosilicate catalysts with 3D structure for benzylation of aromatics," *Catalysis Today*, vol. 204, pp. 125–131, 2013.